Superhydrophobic Behavior of a Perfluoropolyether Lotus-Leaf-like Topography

Lei Zhang,[†] Zhilian Zhou,[‡] Bin Cheng,[‡] Joseph M. DeSimone,[†,‡] and Edward T. Samulski*[,†,‡]

Curriculum in Applied & Materials Sciences and Department of Chemistry, University of North Carolina at Chapel Hill, Chapel Hill, North Carolina 27599-3290

Received May 17, 2006. In Final Form: June 30, 2006

We demonstrate the fabrication of 2-D arrays of nanopillars made from perfluoropolyether derivatives using a porous anodic aluminum oxide membrane as a template. Pretexturing the aluminum prior to anodization enables one to engineer multiple morphological length scales and thereby synthesize a lotus-leaf-like topography. Both nanopillars on a flat surface and on a lotus-leaf-like topology exhibit superhydrophobicity, low contact angle hysteresis, and self-cleaning.

Introduction

The lotus effect,[1] a water droplet rolling down a lotus leaf while removing superficial dirt particles along its way, has captured the attention of many materials scientists recently as there are potential applications ranging from self-cleaning (building exteriors, windshields, and fabrics)[2−4] to reduced-friction surfaces for microfluidic channels.[5] These phenomena derive from the lotus leaf's unusual surface topography,[1,6,7] micrometer-scale protuberances decorated with nanometer-sized hair- or flakelike fine structures in conjunction with a hydrophobic epicuticular wax layer on the leaf surface (Figure 1). The lotus leaf's multiscale topographic surface exhibits superhydrophobicity—a water droplet contact angle in excess of 150°. In addition to superhydrophobicity, low contact angle hysteresis[8−11] is necessary for the self-cleaning process. Dirt particles on the leaf lie on the tips of the fine protrusions, which in turn have low adhesion forces. Therefore, dirt preferentially adheres to the surface of rolling droplets, and the surface self-cleans.

Considerable effort has been expended on fabricating superhydrophobic and self-cleaning surfaces. According to the Cassie−Baxter equation,[12] both a rough surface and a low surface energy material are prerequisite for a high contact angle, so generally, most attempts to fabricate such surfaces fall into the two categories.[13] One centers around methods that cover a rough surface with a low surface energy material; the second involves roughening of a surface of hydrophobic materials. The normal

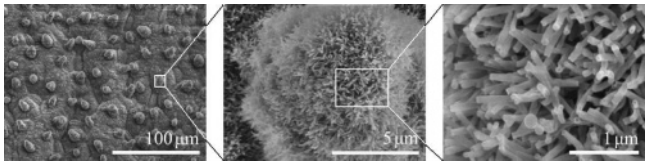

Figure 1. FE-SEM images of the surface structures of *Rosa Plena* lotus leaf at different magnifications, scale bars 100, 5, and 1 μm, respectively. Note the multiscale features ranging from ∼10 μm to ∼100 nm, which are necessary for the superhydrophobic lotus effect.

ways to generate rough surfaces include electrospinning,[14,15] template methods,[16−18] plasma, reactive ion, or chemical etching,[8,11,19] chemical vapor deposition,[20−22] electrodeposition,[23,24] nanorod array growth,[25] polymer solution evaporation,[26] and textured block copolymer morphologies.[27,28] Low surface energy coating materials include poly(tetrafluoroethylene),[22] semifluorinated silanes,[29,30] fluorinated copolymers,[31] and aliphatic thiols.[23] Most of the methods disclosed to date require multistep

* To whom correspondence should be addressed. Fax: (919) 962-2388. Phone: (919) 962-1561. E-mail: et@unc.edu.

[†] Curriculum in Applied & Materials Sciences.

[‡] Department of Chemistry.

(1) Barthlott, W.; Neinhuis, C. *Planta* **1997**, *202*, 1−8.
(2) Callies, M.; Quere, D. *Soft Matter* **2005**, *1*, 55−61.
(3) Quere, D. *Nat. Mater.* **2002**, *1*, 14−15.
(4) Nakajima, A.; Hashimoto, K.; Watanabe, T. *Monatsh. Chem.* **2001**, *132*, 31−41.
(5) Choi, C.-H.; Kim, C.-J. *Phys. Rev. Lett.* **2006**, *96*, 066001.
(6) Furstner, R.; Barthlott, W.; Neinhuis, C.; Walzel, P. *Langmuir* **2005**, *21*, 956−961.
(7) Cheng, Y.-T.; Rodak, D. E. *Appl. Phys. Lett.* **2005**, *86*, 144101.
(8) Oner, D.; McCarthy, T. J. *Langmuir* **2000**, *16*, 7777−7782.
(9) Chen, W.; Fadeev, A. Y.; Hsieh, M. C.; Oner, D.; Youngblood, J.; McCarthy, T. J. *Langmuir* **1999**, *15*, 3395−3399.
(10) Quere, D.; Lafuma, A.; Bico, J. *Nanotechnology* **2003**, *14*, 1109−1112.
(11) Krupenkin, T. N.; Taylor, J. A.; Schneider, T. M.; Yang, S. *Langmuir* **2004**, *20*, 3824−3827.
(12) Cassie, A. B. D.; Baxter, S. *Trans. Faraday Soc.* **1944**, *40*, 546−551.
(13) Feng, L.; Li, S.; Li, Y.; Li, H.; Zhang, L.; Zhai, J.; Song, Y.; Liu, B.; Jiang, L.; Zhu, D. *Adv. Mater.* **2002**, *14*, 1857−1860.
(14) Ma, M.; Hill, R. M.; Lowery, J. L.; Fridrikh, S. V.; Rutledge, G. C. *Langmuir* **2005**, *21*, 5549−5554.
(15) Jiang, L.; Zhao, Y.; Zhai, J. *Angew. Chem., Int. Ed.* **2004**, *43*, 4338−4341.
(16) Feng, L.; Li, S.; Li, H.; Zhai, J.; Song, Y.; Jiang, L.; Zhu, D. *Angew. Chem., Int. Ed.* **2002**, *41*, 1221−1223.
(17) Jin, M.; Feng, X.; Feng, L.; Sun, T.; Zhai, J.; Li, T.; Jiang, L. *Adv. Mater.* **2005**, *17*, 1977−1981.
(18) Feng, L.; Song, Y.; Zhai, J.; Liu, B.; Xu, J.; Jiang, L.; Zhu, D. *Angew. Chem., Int. Ed.* **2003**, *42*, 800−802.
(19) Youngblood, J. P.; McCarthy, T. J. *Macromolecules* **1999**, *32*, 6800−6806.
(20) Li, H.; Wang, X.; Song, Y.; Liu, Y.; Li, Q.; Jiang, L.; Zhu, D. *Angew. Chem., Int. Ed.* **2001**, *40*, 1743−1746.
(21) Li, S.; Li, H.; Wang, X.; Song, Y.; Liu, Y.; Jiang, L.; Zhu, D. *J. Phys. Chem. B* **2002**, *106*, 9274−9276.
(22) Lau, K. K. S.; Bico, J.; Teo, K. B. K.; Chhowalla, M.; Amaratunga, G. A. J.; Milne, W. I.; McKinley, G. H.; Gleason, K. K. *Nano Lett.* **2003**, *3*, 1701−1705.
(23) Jiang, Y.; Wang, Z.; Yu, X.; Shi, F.; Xu, H.; Zhang, X. *Langmuir* **2005**, *21*, 1986−1990.
(24) Zhao, N.; Shi, F.; Wang, Z.; Zhang, X. *Langmuir* **2005**, *21*, 4713−4716.
(25) Feng, X.; Feng, L.; Jin, M.; Zhai, J.; Jiang, L.; Zhu, D. *J. Am. Chem. Soc.* **2004**, *126*, 62−63.
(26) Erbil, H. Y.; Demirel, A. L.; Avci, Y.; Mert, O. *Science* **2003**, *299*, 1377−1380.
(27) Han, J. T.; Xu, X.; Cho, K. *Langmuir* **2005**, *21*, 6662−6665.
(28) Minko, S.; Muller, M.; Motornov, M.; Nitschke, M.; Grundke, K.; Stamm, M. *J. Am. Chem. Soc.* **2003**, *125*, 3896−3900.
(29) Zhai, L.; Cebeci, F. C.; Cohen, R. E.; Rubner, M. F. *Nano Lett.* **2004**, *4*, 1349−1353.
(30) Miwa, M.; Nakajima, A.; Fujishima, A.; Hashimoto, K.; Watanabe, T. *Langmuir* **2000**, *16*, 5754−5760.
(31) Yabu, H.; Takebayashi, M.; Tanaka, M.; Shimomura, M. *Langmuir* **2005**, *21*, 3235−3237.

10.1021/la061400o CCC: $33.50
Published on Web 08/31/2006

fabrication or surface treatments, many of the fabricated superhydrophobic surfaces are not flexible, and some of them are not translucent, which limits applications.

Recently, DeSimone and co-workers reported the fabrication of solvent-resistant photocurable perfluoropolyethers,[32,33] which are low surface tension liquids at room temperature and solidify on UV irradiation (prepolymer cross-linking). Cross-linked perfluoropolyethers exhibit low surface energy, high gas permeability, low toxicity, and extremely high chemical stability, like Teflon, which makes this material an ideal coating.

The use of a porous anodic aluminum oxide (p-AAO) membrane as a template or mold for nanomaterial fabrication is widely applied.[34] The parameters of a p-AAO membrane (such as membrane thickness, pore diameter, and spacing) which determine the ultimate characteristics of the molded nanomaterials are easily controlled by changing the anodization voltage, time, and posttreatment. A wide range of nanomaterials[35−39] including nanofibers or nanorods composed of metals, metal oxides, carbon, polymers, or composites have been fabricated using p-AAO membrane molds. The fabricated nanomaterials are uniform, and if it is contiguous on the exterior of the mold, a well-aligned array of nanostructures can be fabricated.[40]

In the present paper, we report the preparation of flexible, translucent, and stable superhydrophobic films made of cross-linked styrene end-functionalized perfluoropolyether (PFPE) and a highly fluorinated styrene sulfonate ester (SS) that has a nanopillar structure or a lotus-leaf-like topography. The multiscale topography on the PFPE−SS film is made via a relatively simple process: UV radiation of the prepolymer using a textured p-AAO membrane as a mold. Contact angle measurements show that the fabricated film exhibits superhydrophobic characteristics with a low contact angle hysteresis. Theoretical calculations indicate that a water droplet on the PFPE−SS fine structure (nanopillars) is in a Cassie state:[41] the droplet is lying on top of the lattice of nanopillars.

Experimental Section

To make a p-AAO membrane, a high-purity aluminum foil (99.99%) was anodized in a homemade Teflon cell. One surface of the aluminum foil was in contact with a copper anode, and the other one was exposed to the electrolyte, a 0.3 M phosphoric acid aqueous solution; a platinum wire served as the cathode. The Teflon cell was placed in a refrigerated circulating bath, and the electrolyte was vigorously stirred to avoid local heating at the interface of the aluminum and aluminum oxide. The aluminum foil was anodized at 180 V at 2 °C following the well-known two-step anodization procedure.[42−44] A range of p-AAO membranes with different membrane thicknesses can be achieved by controlling the anodization time. After formation, p-AAO membranes were immersed in 5% phosphoric acid aqueous solution for a 40 min posttreatment at 30 °C for pore enlargement. Last, p-AAO membranes were cleaned with water and dried in air for future use.

The low modulus of the originally reported photocurable perfluoropolyether[32] (8 MPa) makes it rather difficult to remove from the p-AAO mold. Typically the p-AAO has 140 nm diameter pores that are several micrometers in length (the thickness of the anodized layer). By using a styrene end-functionalized PFPE and copolymerizing it with a highly fluorinated styrene sulfonate ester, the resulting cross-linked PFPE−SS exhibits a higher modulus (114 MPa) while keeping all the other advantages of PFPE. (The detailed procedure of the preparation of the PFPE−SS precursor material will be published elsewhere.[45])

PFPE and SS precursors were mixed with a weight ratio of 40% to 60% at 80 °C and cured on the surface of a p-AAO membrane using UV light under an Ar atmosphere. The prepolymer infiltrates the template and yields, after it is peeled off, a low surface energy (inverted) replica of the template membrane mold, i.e., an array of nanopillars with diameters and heights determined by the p-AAO membrane template.

A lotus-leaf-like topography with multiple structural scales composed of the low surface energy PFPE−SS elastic network can be fabricated using a modest variation on the template method. The fabrication process is outlined here and in Figure 2. A glass slide was first immersed in 0.3 M sulfuric acid aqueous solution at 90 °C overnight.[46,47] The treated glass was cleaned using distilled water and dried with compressed air. An appropriate amount of 20 μm glass spheres (Duke Cooperation Co.) was dispersed in ethanol and the suspension was placed onto the surface of the glass slide. Under a delicate process of vibration with solvent evaporation, a monolayer of glass spheres is obtained on the surface of the glass slide. By pressing the monolayer of spheres on the glass into the aluminum foil using a hydraulic press[48] (PHI melt press) under a pressure of approximately 3200 kg cm^{-2}, an array of concave features—the negative replica of the close-packed glass spheres—was embossed into the surface of the aluminum. The glass spheres can be removed from the dimpled aluminum surface by sonication. Following the same anodization procedure, the dimpled aluminum develops a honeycomb of porous channels in the conformal p-AAO membrane; the hexagonal pores are normal to the hemispherical dimples. Similar to the conventional flat p-AAO template method, the liquid mixture of PFPE and SS precursors was added to the patterned porous surface of the membrane and cured under an Ar atmosphere with UV irradiation. Afterward, the cross-linked PFPE−SS film was peeled off of the textured p-AAO template, and contact angles were measured.

Morphology characterization was carried out using an FE-SEM instrument (Hitachi S4700). A thin layer of gold (around 10 nm thick) was coated onto the surface of PFPE−SS samples using a sputter coater (Cressington 108 auto) to obtain high-quality images. Water contact angle measurement was done using a KSV CAM200 contact angle goniometer, and 32-bit Windows-based KSV CAM software based on the true Young & Laplace equation allows extraction of the contact angles.

Results and Discussion

Figure 3A is the top view FE-SEM image of the as-prepared p-AAO membrane which was made by anodizing aluminum foil in 0.3 M phosphoric acid aqueous solution at 2 °C for 20 min; the pores were enlarged in 5% phosphoric acid aqueous solution at 30 °C for 40 min. The pores are approximately hexagonally

(32) Rolland, J. P.; Van Dam, R. M.; Schorzman, D. A.; Quake, S. R.; DeSimone, J. M. *J. Am. Chem. Soc.* **2004**, *126*, 2322−2323.
(33) Wood, C. D.; Michel, U.; Rolland, J. P.; DeSimone, J. M. *J. Fluorine Chem.* **2004**, *125*, 1671−1676.
(34) Martin, C. R. *Science* **1994**, *266*, 1961−1966.
(35) Xu, T. T.; Fisher, F. T.; Brinson, L. C.; Ruoff, R. S. *Nano Lett.* **2003**, *3*, 1135−1139.
(36) Che, G.; Lakshmi, B. B.; Martin, C. R.; Fisher, E. R. *Chem. Mater*. **1998**, *10*, 260−267.
(37) Steinhart, M.; Wendorff, J. H.; Greiner, A.; Wehrspohn, R. B.; Nielsch, K.; Schilling, J.; Choi, J.; Gosele, U. *Science* **2002**, *296*, 1997.
(38) Kim, K.; Lee, S. H.; Yi, W.; Kim, J.; Choi, J. W.; Park, Y.; Jin, J.-I. *Adv. Mater.* **2003**, *15*, 1618−1622.
(39) Nielsch, K.; Muller, F.; Li, A.-P.; Gosele, U. *Adv. Mater*. **2000**, *12*, 582−586.
(40) Zhang, L.; Cheng, B.; Samulski, E. T. *Chem. Phys. Lett.* **2004**, *398*, 505−510.
(41) Patankar, N. A. *Langmuir* **2004**, *20*, 7097−7102.
(42) Masuda, H.; Fukuda, K. *Science* **1995**, *268*, 1466−1468.
(43) Masuda, H.; Yada, K.; Osaka, A. *Jpn. J. Appl. Phys.* **1998**, *37*, L1340-L1342.
(44) Li, A. P.; Muller, F.; Bimer, A.; Nielsch, K.; Gosele, U. *J. Appl. Phys.* **1998**, *84*, 6023−6026.
(45) Zhou, Z.; Dominey, R. N.; Rolland, J. P.; Maynor, B. W.; Pandya, A. A.; DeSimone, J. M.; *J. Am. Chem. Soc.*, in press, 2006.
(46) Micheletto, R.; Fukuda, H.; Ohtsu, M. *Langmuir* **1995**, *11*, 3333−3336.
(47) Yan, X.; Yao, J.; Lu, G.; Li, X.; Zhang, J.; Han, K.; Yang, B. *J. Am. Chem. Soc.* **2005**, 7688−7689.
(48) Asoh, H.; Nishio, K.; Nakao, M.; Tamamura, T.; Masuda, H. *J. Electrochem. Soc.* **2001**, *148*, B152−B156.

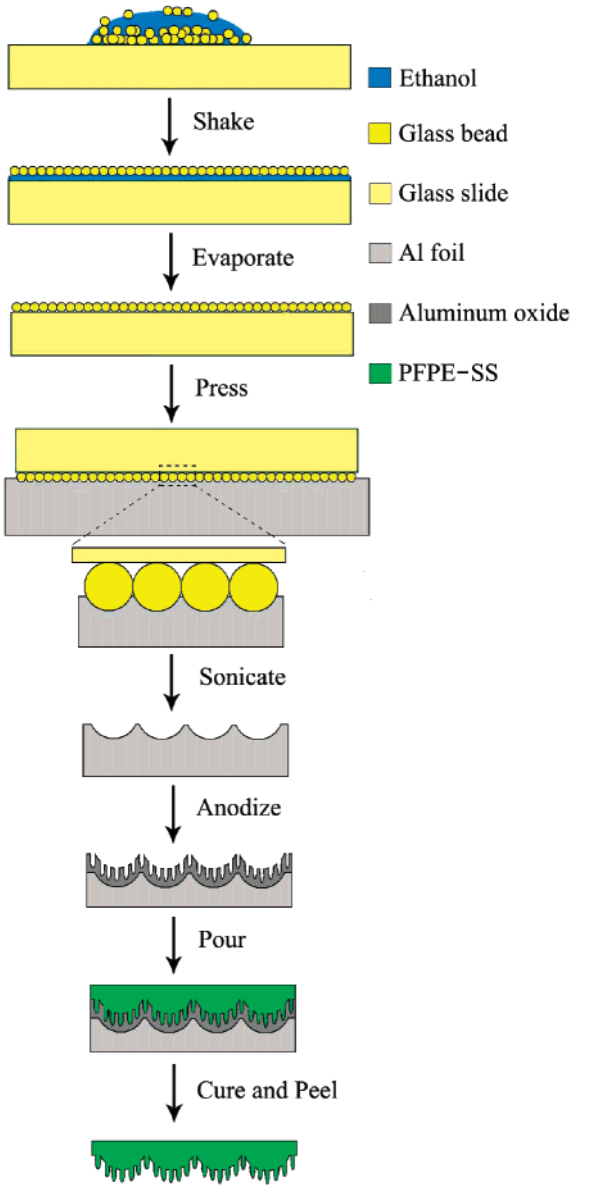

Figure 2. A schematic illustration of the procedure for the fabrication of a lotus-leaf-like PFPE−SS structure.

close-packed with uniform diameters (∼140 nm). Figure 3B shows an oblique (30° angle) view of a cross-section of the p-AAO membrane. The pore channels are straight and parallel with a uniform diameter along the pore length; the pore bottom has a hemispherical shape. The length of the channels is about 3 μm. The FE-SEM image of the PFPE−SS nanopillar film peeled off of the p-AAO membrane is shown Figure 3C. The resulting PFPE−SS nanopillars have an aspect ratio of ∼20, are uniform in length, and have diameters that match the pore diameter. Because of the high aspect ratio and flexibility of polymeric PFPE−SS, the nanopillars collapse into conical bundles. The inset shows a water droplet on the partially bundled PFPE−SS nanopillar surface. Static contact angles as high as 171° were observed.

PFPE−SS nanopillar films with different pillar lengths were fabricated using p-AAO membranes with different thicknesses (anodization times). Figure 4A shows an image of PFPE−SS nanopillars from a p-AAO membrane anodized for 10 min with further pore enlargement for 40 min. The nanopillars, with lengths of around 0.7 μm, are straight and parallel to each other. The tips of the nanopillars are hemispherical, which is the negative replica

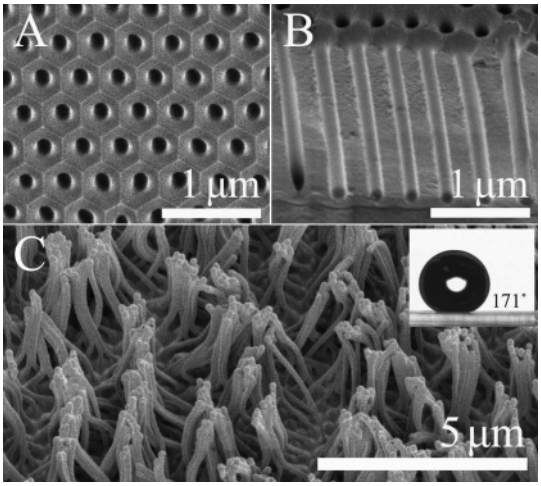

Figure 3. (A) Top view and (B) 30° angle oblique view FE-SEM images of a p-AAO membrane template anodized for 20 min at 180 V. (C) FE-SEM image of a PFPE−SS nanopillar film peeled from the p-AAO membrane. The inset is a water droplet, with an extremely high static contact angle, sitting on the PFPE−SS nanopillars.

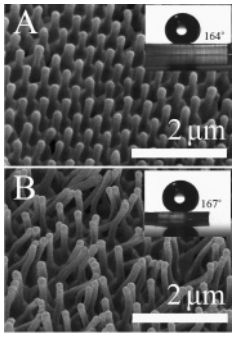

Figure 4. FE-SEM micrographs of PFPE−SS nanopillar films peeled from p-AAO membranes anodized at 180 V for (A) 10 min and (B) 15 min and pore-enlarged in 5% phosphoric acid aqueous solution at 30 °C for 40 min. The inset in the top right corner of each image is the water droplet on the as-prepared PFPE−SS nanopillar film.

of the pore bottom in the p-AAO membrane. A maximum static water contact angle of 164° was observed (inset of Figure 4A). An FE-SEM image of nanopillars nearly 1.5 μm long is shown in Figure 4B. The template was made from a p-AAO membrane anodized for 15 min with pore enlargement for 40 min. Some of the nanopillars are separate, and some of them are aggregated into bundles; this topology is an intermediate state between that shown in Figure 3C and that in Figure 4A. The inset shows the static water contact angle (∼167°).

Although all the PFPE−SS nanopillar surfaces show water contact angles above 150°, which suggests that the as-prepared surfaces possess superhydrophobicity, the status of a water droplet on PFPE−SS nanopillars is not clear. The Cassie−Baxter formula, which gives the apparent contact angle θ_r^c of a droplet on a rough surface (with a surface fraction ϕ_s) in the Cassie state, can give some insights into the situation:

$$\cos \theta_r^c = -1 + \phi_s(\cos \theta + 1) \quad (1)$$

The surface fraction ϕ_s corresponds to the ratio of the actual area of liquid−solid contact to the horizontal projected area of the substrate; θ is the water contact angle on a flat surface having the same chemical composition. For the surface fabricated from a p-AAO membrane anodized for 10 min (Figure 4A), the separated nanopillars are hexagonally close-packed and the tips are hemispherical. A schematic illustration of the unit cell for

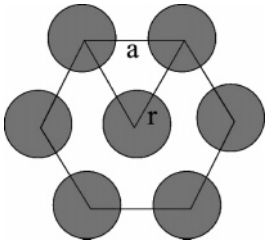

Figure 5. A schematic illustration of the unit cell of hexagonally closed-packed PFPE−SS nanopillars.

this case is shown in Figure 5. If the water droplet only contacts the hemispherical tips of the nanopillars, the value of the surface fraction ϕ_s can be estimated from

$$\phi_s = \frac{3(2\pi r^2)}{6\left(\frac{1}{2}\frac{\sqrt{3}}{2}a^2\right)} \quad (2)$$

where r is the radius of the PFPE−SS nanopillars and a is the interpillar distance. For the PFPE−SS nanopillars in Figure 4A, the radius r is ∼70 nm and the interpillar distance a is ∼400 nm; these parameters yield a value of 0.24 for the surface fraction ϕ_s. The contact angle of the water droplet on a flat PFPE−SS surface is approximately 104°. Therefore, the apparent angle given by the Cassie−Baxter formula is $\theta_r^c = 145°$. However, the actual contact angle, 164°, is much larger. This result requires a much smaller surface fraction. Substituting θ_r^c in the Cassie−Baxter formula with 164°, the required value for the surface fraction ϕ_s* equals 0.052, which is 25% of the surface fraction ϕ_s. Therefore, we infer that the water droplet lies on the tips of the nanopillars with air trapped beneath the pillars. Moreover, the water contacts only 22% of the hemispherical surface of the nanopillars. When the nanopillars are longer and form conelike bundles, this further reduces the contact area between the water droplet and PFPE−SS nanopillars. This, in turn, would further lower the surface fraction and increase the water contact angle. Therefore, the maximum static water contact angle increases as the nanopillar length increases.

The FE-SEM micrographs associated with the different fabrication steps of the multiscale, lotus-leaf-like PFPE−SS structure are shown in Figure 6. Figure 6A shows a FE-SEM image of a monolayer of glass spheres on a glass slide. A uniform area around 1 cm^2 could be readily obtained; Figure 6B is a magnified image of the ∼20 μm glass sphere monolayer. It indicates that the glass spheres are approximately hexagonally close-packed. The dimpled aluminum foil after the glass sphere monolayer was pressed into the aluminum is shown in Figure 6C. After the pressing stage, most of the glass spheres remain embedded in the aluminum foil. Figure 6D shows the FE-SEM micrograph of the dimpled aluminum foil after sonication; all the glass spheres are removed from the aluminum foil surface, and the concave dimples are apparent. Figure 6E shows the FE-SEM image of the honeycomb of pores in the p-AAO membrane (anodized in 0.3 M phosphoric acid aqueous solution at 180 V for 20 min at 2 °C; after the two-step anodization, pore enlargement was conducted in 5% phosphoric acid aqueous solution for 40 min at 30 °C). Figure 6F is a FE-SEM micrograph of the membrane at a larger magnification. Since the aluminum foil retains the micrometer-scale dimples after the two-step anodization, the dimpled structure on the aluminum foil surface does not appear to affect the anodization: the pores are normal to the surface, parallel, and straight. This also explains why the

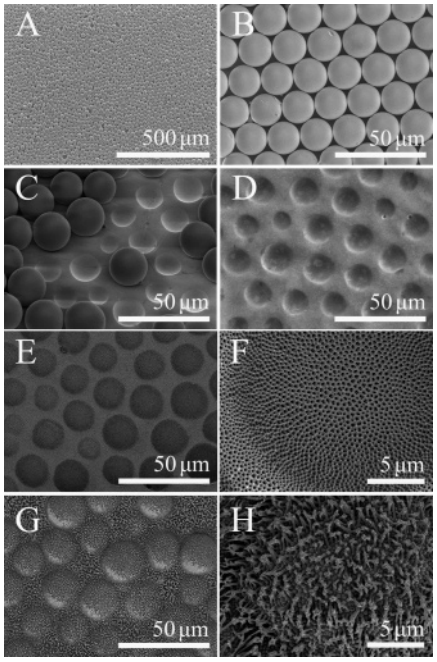

Figure 6. FE-SEM micrographs of (A, B) a glass sphere monolayer at different magnifications, (C) dimpled aluminum foil after the glass spheres were pressed into the aluminum, (D) dimpled aluminum foil after sonication, (E, F) a honeycomb-like p-AAO membrane at different magnifications, and (G, H) a lotus-leaf-like PFPE−SS molded replica at different magnifications.

pore openings at the bottom of the concave dimples appear larger than the foreshortened openings on those oblique surfaces in the top view FE-SEM image. Parts F and H of Figure 6 show the corresponding FE-SEM images of the lotus-leaf-like PFPE−SS structure that is peeled from the porous, dimpled p-AAO membrane. These images clearly show that 20 μm hemispherical "dimples" populating the PFPE−SS are punctuated by hundred nanometer PFPE−SS pillars. This topography has two distinct spatial scales and mimics the lotus leaf surface. It yields a maximum static contact angle of 169°.

Recent studies have suggested that the static contact angle does not reflect the ability of water drops to stick to a substrate[10] and does not adequately describe the hydrophobicity of a surface.[9] In addition to a large contact angle, a low contact angle hysteresis is thought to play an important role in the self-cleaning phenomenon. Contact angle hysteresis is the difference between the advancing and receding contact angle values. Drops exhibit an advancing edge by addition of liquid into the drop on a surface with a microsyringe and a receding edge on withdrawal of the liquid from the drop. Water contact angles of the flat PFPE−SS surface, the PFPE−SS nanopillars on a flat surface from a p-AAO membrane template anodized for 20 min (Figure 3C), and the lotus-leaf-like PFPE−SS topography (Figure 6G) are shown in Table 1. Both the PFPE−SS nanopillars on a flat surface and the lotus-leaf-like topography show a small contact angle hysteresis (∼10°), which is much less than that of a smooth (untextured) PFPE−SS surface. The underlying reason is that the hairlike nanopillars present a discontinuous three-phase contact line with the water droplet, decreasing friction and lowering the energy barrier for the advancing and receding drop.[8,9] When the flat surface comprised of PFPE−SS nanopillars was tilted to ∼3° relative to the horizontal, a 5 mg water droplet began rolling because of gravity. The lotus-leaf-like structured surface also requires a tilt angle of ∼3° for the water droplet to move. This suggests that the adhesion force between the water drop and the multiscale structured PFPE−SS surface is small.

Table 1. Dynamic and Static Contact Angles Measured on a Flat PFPE−SS Surface, PFPE−SS Nanopillars Fabricated Using a Flat p-AAO Membrane Anodized for 20 min (Figure 3C), and a PFPE−SS Lotus-Leaf-like Structure (Figure 6G)[a]

	advancing contact angle (deg)	receding contact angle (deg)	max static contact angle (deg)	tilted angle at which the water droplet begins rolling (deg)
PFPE−SS flat surface	107	73	104	
PFPE−SS nanopillars (Figure 3C)	173	162	171	3
PFPE−SS lotus-leaf-like structure (Figure 6G)	170	160	169	3

[a] Tilted angles at which the water droplet begins to roll are also listed.

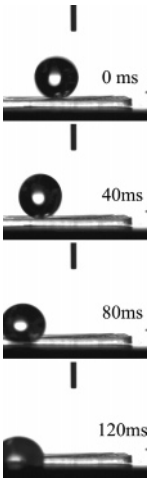

Figure 7. Motion of a water droplet on a flat PFPE−SS film punctuated with nanopillars (Figure 3C) (p-AAO membrane anodized for 20 min at 180 V).

In addition to the static and dynamic contact angle measurements, the dynamic behavior of water on a flat PFPE−SS film punctuated with nanopillars was studied. The dynamics of a water droplet falling onto the surface mimics rain falling onto a lotus leaf. The images shown in Figure 7 were taken with a digital CCN fire-wire camera at a rate of 25 frames per second on a CAM 200 station. A microsyringe attached to a needle with an inner diameter of 0.15 mm and an outer diameter of 0.30 mm was employed to form a water droplet. The tip of the needle was 3.4 mm away from the surface of the PFPE−SS nanopillars, which was tilted approximately 0.5° relative to the horizontal. A water droplet with a 2.2 mm diameter detached from the needle hit the PFPE−SS nanopillar surface and rolled on the PFPE−SS nanopillar surface to the working stage with no hesitation. Fine fibrous debris on the PFPE−SS nanopillared flat surface and the multiscale lotus-leaf-like topography could be removed by the moving water droplet. These observations are reminiscent of the water-repellant lotus leaf and the process of self-cleaning.

Conclusions

p-AAO membranes fabricated using the two-step aluminum anodization process yield superhydrophobic films punctuated with PFPE−SS nanopillars having controllable aspect ratios. A PFPE−SS topography that mimics the multiscale roughness of a lotus leaf surface was obtained by a simple UV-induced cross-linking reaction of a low surface energy prepolymer on a textured p-AAO template. The PFPE−SS nanopillars with lengths of ∼3 μm and with "one" (a flat substrate) or mutiple (microdimples punctuated with nanopillars in a lotus-leaf-like topography) spatial scale structures show superhydrophobicity, low contact angle hysteresis, and self-cleaning. While this suggests that multiple length scales may not be essential for superhydrophobicity, it should be emphasized that there are, in fact, multiple length scales when sufficiently long nanopillars created on a flat surface aggregate into separated bundles (Figure 3C).

Acknowledgment. This work is mainly supported by the NASA University Research, Engineering and Technology Institute on Bio Inspired Materials (BIMat) under Award No. NCC-1-02037. We also thank the Department of Energy (Grant 5-35908), NSF Science and Technology Center (Grant 5-37503), and Office of Naval Research (Grant 5-35747) for partial financial support of this project. We thank Dr. Mark H. Schoenfisch for sharing the KSV CAM200 contact angle goniometer.

LA061400O